Open access • Posted Content • DOI:10.1101/2020.03.06.981373

Evidence for oligodendrocyte progenitor cell heterogeneity in the adult mouse brain

Rebecca M. Beiter, Anthony Fernandez-Castaneda, Courtney Rivet-Noor, Andrea Merchak ...+6 more authors

Institutions: University of Virginia

Published on: 08 Mar 2020 - bioRxiv (Cold Spring Harbor Laboratory)

Topics: Population

Evidence for oligodendrocyte progenitor cell heterogeneity in the adult mouse brain.

Authors: Rebecca M. Beiter[1,2], Anthony Fernández-Castañeda[1,2], Courtney Rivet-Noor[1,2], Andrea Merchak[1,2], Robin Bai[1], Erica Slogar[1], Scott M. Seki[1,2,3], Dorian A Rosen[1,4], Christopher C. Overall[1,5], and Alban Gaultier[1,5,#]

[1]Center for Brain Immunology and Glia, Department of Neuroscience, [2]Graduate Program in Neuroscience, [3]Medical Scientist Training Program, [4]Graduate Program in Pharmacological Sciences School of Medicine, University of Virginia, Charlottesville, VA 22908, USA.

[#]Corresponding author. Email: ag7h@virginia.edu

[5]Christopher C. Overall and Alban Gaultier are co-senior authors

ABSTRACT

Oligodendrocyte progenitor cells (OPCs) are a mitotically active population of glia that comprise approximately 5% of the adult brain. OPCs maintain their proliferative capacity and ability to differentiate in oligodendrocytes throughout adulthood, but relatively few mature oligodendrocytes are produced following developmental myelination. Recent work has begun to demonstrate that OPCs likely perform multiple functions in both homeostasis and disease, and can significantly impact behavioral phenotypes such as food intake and depressive symptoms. However, the exact mechanisms through which OPCs might influence brain function remains unclear. In this work, we demonstrate that OPCs are transcriptionally diverse and separate into three distinct populations in the homeostatic brain. These three groups show distinct transcriptional signatures and enrichment of biological processes unique to individual OPC populations. We have validated these OPC populations using multiple methods, including multiplex RNA in situ hybridization and RNA flow cytometry. This study provides an important resource that profiles the transcriptome of adult OPCs and will provide a significant foundation for further investigation into novel OPC functions.

INTRODUCTION

First described in the early 1980's, oligodendrocyte progenitor cells (OPCs) are the fourth major glial subtype present in the brain. Depending on the region examined, OPCs makeup anywhere from 2-8% of the adult central nervous system (CNS) cells.[1,2]. Adult OPCs belong to the same population of progenitors that give rise to oligodendrocytes during CNS development. However, a large fraction of OPCs do not differentiate, but instead remain in a progenitor state throughout adulthood, a property not consistent with the relatively small need to generate new oligodendrocytes[2-6]. While it has been demonstrated that the differentiation of OPCs into myelinating oligodendrocytes is critical for processes such as motor learning during adulthood, recent evidence indicates that mature oligodendrocytes are a relatively stable population in the adult brain[7-9]. The slow rate at which oligodendrocytes are replaced throughout life does not correlate with the maintenance of a highly dynamic and energetically costly population of OPCs[7,8,10]. With this discordance between the dynamics of the OPC population and the relatively small need for newly differentiated oligodendrocytes in adulthood, the field has begun to explore alternate functions of adult OPCs[11,12].

Under homeostatic conditions, OPCs express distinct ion channel profiles that vary with both the brain region and developmental stage of the organism, indicating that subpopulations of OPCs maintain unique electrical properties and therefore may be performing multiple functions within the brain[13]. Furthermore, loss of OPCs, either globally or regionally, has been shown to result in significant depressive-like behavior, persistent weight-gain and leptin-insensitivity, as well as microglial activation and subsequent neuronal death[14-16]. In pathological conditions, OPCs can upregulate cytokine production in response to IL-17 signaling and greatly contribute to CNS pathogenesis[17]. Surprisingly, OPCs also upregulate antigen presentation machinery in the demyelinating CNS, and can regulate T cell function[18-20]. Taken together, these studies illustrate the dynamic role OPCs can play in the adult CNS and build a strong case in support of exploring adult OPCs diversity at the transcriptional level. Such an overview will provide an important resource for further functional investigation of OPCs in the CNS.

Here, we have developed an inducible OPC reporter mouse strain, which expresses YFP in PDGFRα-expressing cells after tamoxifen administration. After extensive validation, we used this tool to isolate OPCs from the adult brain by fluorescent activated cell sorting (FACS) and perform single-cell sequencing. We demonstrate the presence of three novel populations of transcriptionally distinct OPCs in the adult brain. Gene Ontology (GO) term analysis and gene expression analysis of identified OPC subtypes suggest specialization of OPCs, encompassing potential functions such as immune system modulation and neuronal regulation. Sequencing results were further validated by measuring co-expression of canonical OPC markers along with cluster-specific genes identified from our sequencing dataset using RNAscope and qPCR. Taken together our results present a unique toolbox to support functional exploration of OPCs under homeostatic and pathological conditions.

METHODS

Animals

PDGFRα-Cre^{ER} mice (Jackson #018280) were crossed to R26-EYFP (Jackson, #006148) animals to generate PDGFRα-Cre^{ER}; R26-EYFP, a previously described model[21]. C57B/6J were purchased from Jackson. Mice were maintained on a 12 hours light/dark cycle with lights on at 7am. Behavior was performed on mice used in single-cell sequencing run 1. Testing consisted of sucrose preference, elevated plus maze, open field, and forced swim test. All animal experiments were approved and complied with regulations of the Institutional Animal Care and Use Committee at the University of Virginia (#3918).

Tamoxifen injections

Tamoxifen (C8267, Sigma-Aldrich) was dissolved in corn oil at 37°C overnight at 20 mg/ml. Tamoxifen was administered *i.p*. at 200 mg/kg with a maximum dose of 4 mg per injection. For single-cell sequencing experiments, 6 week old mice were given 2 injections of tamoxifen 3 days apart. For validation of Cre recombination in PDGFRα-Cre$^{ER;}$ R26-EYFP brains, 5-6 week old mice were injected with 0, 1, 2, or 3 doses of tamoxifen, each given three days apart. For those mice receiving three doses of tamoxifen, the final dose was given at 150 mg/kg.

Immunofluorescence

Mice were deeply anesthetized with pentobarbitol and subsequently perfused with 5 units/Ml heparin in saline followed by 10% buffered formalin, each for approximately 1 minute. For brain tissue, brains were rapidly dissected and post-fixed in 10% buffered formalin overnight at 4°C. Tissue was then transferred into 30% sucrose in PBS and allowed to sink for at least 24 hours. Brains were frozen in OCT, sectioned, and stored in PBS+0.02% NaAz until further staining.

Tissue was blocked with PBS, 1% BSA, 0.5% Triton-X 100, 2% normal donkey serum, and 1:200 CD16/CD32 (14-0161-82, 1:200, eBioscience) for at least 1 hour at room temperature. For stains utilizing a mouse primary antibody, tissue was blocked in Mouse

on Mouse Blocking Reagent (MKB-2213, Vector Laboratories) according to manufacturer's instructions for at least 1 hour at room temperature. Tissue was incubated in primary antibodies overnight at 4°C with gentle agitation. Tissue was washed three times in TBS and 0.3% Triton-X 100 and incubated in secondary antibodies overnight at 4°C with gentle agitation. Following secondary incubation, tissue was stained with Hoechst (1:700, ThermoFisher Scientific, H3570) for 10 minutes at room temperature, washed 3 times TBS and Triton-X 100, and mounted on slides using Aqua Mount Slide Mounting Media (Lerner Laboratories). Images were collected on a Leica TCS SP8 confocal microscope and processed using Fiji.

Antibodies for Immunofluorescence

Primary antibodies used for immunofluorescence were PDGFRα (1:200, R&D Systems, AF1062), Olig2 (1:200, Millipore, MABN50), GFP-488 (1:400, Fisher Scientific, A21311), and GFP (1:1000, Invitrogen, A10262). Secondary antibodies used were Donkey anti-Goat Cy3 (2µg/mL, Jackson ImmunoResearch, 705-165-147), Donkey anti-Mouse 647 (2µg/mL, Jackson ImmunoResearch, 715-605-150), Donkey anti-Mouse 546 (2µg/mL, Life Technologies, A10036), Donkey anti-Chicken 488 (2µg/mL, Jackson ImmunoResearch, 703-545-155), and Donkey anti-Goat 647 (2µg/mL, Invitrogen, A21447).

Isolation of CNS cells

To prepare cells for single-cell sequencing, adult mice (8-20 weeks) were anesthetized with pentobarbitol and subsequently perfused with 5 units/ml heparin in saline for approximately 1 minute. Brains were rapidly dissected and finely minced. Tissue was digested in HBSS with calcium and magnesium (Gibco, 14025-092) supplemented with 20 units per mL papain (Worthington Biochemical LS003126) and 50 units per mL DNase (Worthington Biochemical, LS002139) for single-cell sequencing experiments. For OPC cluster sorting, tissue was digested in HBSS with calcium and magnesium (Gibco, 14025-092) supplemented with 7.5-20 units per mL papain (Worthington Biochemical LS003126) and 50 units per mL DNase (Worthington Biochemical, LS002139) or DMEM (Gibco, 11965-092) supplemented with 1mg/ml collagenase VIII (Sigma, C2139) and 50 units per

mL DNase (Worthington Biochemical, LS002139). Tissue was digested at 37°C with gentle shaking for 45 minutes, with trituration after every 15-minute interval to dissociate the tissue. Following digestion, a 40% Percoll gradient (GE Healthcare, 17-0891-01) was used to remove myelin and other debris from the samples. Resulting single-cell suspensions from 4-5 mice were pooled for each sequencing sample and subsequently stained for FACS sorting.

FACS sorting

For single-cell sequencing experiments, single-cell suspensions were stained for 30 minutes at room temperature with the following antibodies: O4-APC (O4, 10µL/test, Miltenyi, 130-095-891), CD11b-e450 (M1/70, 0.5 µL/test, eBioscience, 48-0112-82), TER119-APC/Cy7 (TER-119, 1.25 µL/test, Biolegend, 116223), PDGFRα-PE/Cy7 (APA5, 0.625 µL/test, Invitrogen, 25-1401-82), CD45-PerCP/Cy5.5 (30-F11, 0.5 µL/test, eBioscience, 45-0451-82), and CD16/31 (93, 0.5 µL/test, Invitrogen, 14-0161-82). Viability was determined using Ghost Dye Violet 510 (0.5 µL/test, Tonbo biosciences, 13-0870). Cells were sorted using a 16-color BD influx cell sorter. Cells sent for sequencing were gated on live/singlets/TER119-/CD45-/CD11b-/YFP+. Following sorting, cells were washed three times with 0.04% BSA and then processed for sequencing according to the 10x Genomics protocol.

For sorting of individual OPC clusters, single-cells suspensions were stained for 30 minutes with CD45-PerCP/Cy5.5 (30-F11, 0.5 µL/test, eBioscience 45-0451-82 or BD Pharmingen 550994), CD16/31 (93, 0.5 µL/test, Invitrogen, 14-0161-82), Ghost Dye Violet 510 (0.5 µL/test, Tonbo biosciences,13-0870), and an antibody against one of the following: Decorin (20µg/test, Invitrogen, PA5-13538), Neurexin 1 (2µg/test, Invitrogen, PA5-79764), or Aquaporin 1 (3µg/test, Invitrogen, PA5-78805). Samples were then stained with Donkey anti-Rabbit 647 (0.2 µg/test, Jackson ImmunoResearch, 711-605-152) or Donkey anti-Rabbit 647 (0.125 µg/test, Biolegend, 406414) for 30 minutes at room temperature. Cells were sorted using a 16-color BD Influx cell sorter. All cells were gated on Live/scatter/singlets/CD45-/YFP+ with an additional gate for Decorin+, Neurexin1+, or

Aquaporin1+ cells. Following sorting, cells were spun down and stored at -80°C until RNA extraction.

Single-Cell Sequencing and Analysis

Library Preparation and Sequencing

Samples were processed for single-cell sequencing according to manufacturer's instructions using the Chromium Next GEM Single-cell 3' Reagent Kit (10xGenomics) and Chromium Controller (10xGenomics). Single-cell libraries were sequenced using the NextSeq 500 Sequencing System (Illumina). Library preparation and sequencing was completed by the Genome Analysis and Technology Core at the University of Virginia.

Quantification

All steps of the quantification process were performed with Cellranger. The fastq files for the samples were quantified using the mkfastq utility, and were quantified against the mm10 mouse genome with the count utility.

Pre-processing

We used Seurat for the single-cell analysis[22,23], and for each of the healthy brain datasets, we followed the same procedure. First, we performed a QC step to identify and remove cells that were potential outliers. This included removing potential multiplets (i.e., cells that had clear outlier gene expression) and cells that had approximately ten percent or more of mitochondrial gene expression (i.e., cells that were likely to have high technical variation). After filtering out these suspect cells, we then normalized and log-transformed the data (using the 'LogNormalize' method), regressed out unwanted sources of technical variation (i.e., the number of detected molecules and mitochondrial contribution to gene expression) [24], and scaled the counts.

Integration

To make comparative analyses possible between the healthy brain datasets, we integrated the datasets with Seurat using the alignment strategy described previously[22]. The first step was to select the genes to be used as the basis for the alignment. Here we

took the union of the 1000 genes with highest variability in each of the datasets, and then filtered this down to only those genes found in each of the datasets, giving us 2,285 genes for the alignment. Next, we identified common sources of variation between the six datasets (3 sequencing runs with 2 samples each) by running a canonical correlation analysis (CCA) with the highly variable genes as features. By examining the strength of the thirty calculated canonical correlations (CCs), we found that the first twelve CCs were driving the variation between the datasets. We then aligned the subspaces [22] (i.e., the first twelve CCs), giving us an integrated dataset with features on a common scale.

Analysis

We then used Seurat on the aligned dataset to identify eight clusters of cells, and then used t-SNE to visualize the similarity between cells. Next, we assigned cell types to these clusters based upon the expression of pre-defined marker genes, and then identified cluster markers by finding the differentially expressed genes in one cluster compared to all other clusters (one-vs-all). Using the gene markers for each cluster, we then used gene set analysis (Fisher's exact test, as implemented in the clusterProfiler Bioconductor package[25]) to identify GO gene sets that were enriched. To better identify markers that differentiated the three OPC clusters from each other, we excluded the other five non-OPC clusters, and then compared each OPC cluster to the other two individually (one-vs-all) and identified the differentially expressed genes. As before, we used these marker genes to identify GO gene sets that were functionally enriched. All analyzed single-cell sequencing data has been uploaded in a searchable database located at http://165.22.7.10:3838/seurat_viewer/seurat_viewer_4.Rmd.

RNAscope

C57B/6J mice (8-10 weeks) from Jackson were anesthetized with pentobarbitol and subsequently perfused with ice-cold 5 units/ml heparin in saline for approximately 1 minute. Brains were rapidly dissected, flash frozen in OCT (Fisher Healthcare, 4585), and stored at -80°C until further processing. Frozen tissue was cut sagittally (15μm), immediately slide-mounted, allowed to dry for approximately 1 hour at -20°C and then stored at -80°C. All tissue was used within three months of dissection.

Tissue was processed using the RNAscope Fluorescent Multiplex Reagent Kit (Advanced Cell Diagnostics, 320850) according to manufacturer's instructions. Briefly, tissue was fixed for 15 minutes in 10% buffered formalin (Fisher Scientific, 23-245685) at 4°C, dehydrated, and then incubated in Protease IV (Advanced Cell Diagnostics, 320850) at room temperature for 30 minutes. Target probes were hybridized to the tissue for 2 hours at 40°C, followed by hybridization of AMP1-FL (30 minutes, 40°C), AMP2-FL (15 minutes, 40°C), AMP3-FL (30 minutes, 40°C), and AMP4-FL (15 minutes, 40°C). Samples were counterstained with supplied DAPI or Hoechst 33342 (1:700, ThermoFisher Scientific, H3570) and mounted on slides using ProLong Glass Antifade Mountant (ThermoFisher, P36980). The following target probes were used: *Olig1* (Advanced Cell Diagnostics, 480651-C2), *Olig2* (Advanced Cell Diagnostics, 447091-C2), *Pdgfrα* (Advanced Cell Diagnostics, 480661), *Clusterin* (Advanced Cell Diagnostics, 427891-C3), *Gpr17* (Advanced Cell Diagnostics,318131-C3), *Cspg4* (Advanced Cell Diagnostics, 404131), *Lumican* (Advanced Cell Diagnostics, 480361-C3), RNAscope 3-plex Positive Control Probes (Advanced Cell Diagnostics, 320881), and RNAscope 3-plex Negative Control Probes (Advanced Cell Diagnostics, 320871). Sections were imaged using a Leica TCS SP8 confocal microscope.

RNAscope Quantification

Following imaging, max projected confocal images were analyzed using CellProfiler Software. RNA expression per cell was quantified using a modified version of a previously published pipeline[26]. Briefly, automated steps were used to draw nuclear masks and subsequently quantify the number of RNA puncta from each channel that colocalized with each nuclear mask. Threshold values for each channel were set based negative control images. Automatic nuclear identification was reviewed and any nuclear mask that clearly contained a large group of nuclei or was located on the edge of an image such that part of the nuclei was not visible was excluded from further analysis. Cells were considered positive for an OPC marker (*Pdgfra*, *Cspg4*, *Olig1*, or *Olig2*) if 4 or more puncta colocalized with a particular nucleus to account for background in the assay[27]. OPCs were defined by the co-expression of two canonical OPC transcripts encoding for cell surface

markers (*Pdgfra* or *Cspg4*) and oligolineage transcription factors (*Olig1* or *Olig2*). The number of transcripts of cluster markers *Clu*, *Lum*, or *Gpr17* were recorded for each identified OPC.

RT-qPCR

RNA was extracted from sorted cell populations using the ISOLATE II RNA Micro Kit (Bioline, BIO-52075). All isolated RNA was reverse transcribed using the SensiFAST cDNA Synthesis Kit (Bioline, BIO-65054). RT-qPCR was performed using the SensiFAST Probe No-ROX Kit (Bioline, BIO-86005) and TaqMan probes for *Gapdh* (ThermoFisher, Mm99999915_g1), *Olig1* (ThermoFisher, Mm00497537_s1), *Olig2* (ThermoFisher, Mm01210556_m1), *Pdgfra* (ThermoFisher, Mm00440701_m1), and *Cspg4* (ThermoFisher, Mm00507257_m1). Data was collected using the CFX384 Real-Time System (Bio-rad).

RNA Flow Cytometry

Cells were isolated from the brains of C57B/6J mice (9-16 weeks, males) according to the same protocol used for single-cell sequencing. Digestion buffer was comprised of HBSS with calcium and magnesium (Gibco, 14025-092) supplemented with 10 units per mL papain (Worthington Biochemical LS003126) and 50 units per mL DNase (Worthington Biochemical, LS002139). Cells were stained with CD45-e450 (0.5 µL/test, Invitrogen, 48-0451-82), CD16/31 (93, 0.5 µL/test, Invitrogen, 14-0161-82), and Ghost Dye Violet 510 (0.5 µL/test, Tonbo biosciences, 13-0870) for 20-30 minutes at room temperature. Cells were subsequently processed for RNA staining according to manufacturer's instructions using the PrimeFlow RNA Assay Kit (ThermoFisher Scientific, 88-18005-204). Cells were incubated with probes targeting *Olig2* (Affymetrix, VPFVKKV-210), *Gpr17* (Affymetrix, VPGZE6T-210), *Clu* (Affymetrix, VB10-3283998-210) and *Pdgfra* (Affymetrix, VB6-3197712-210). A probe targeting *Actb* (Affymetrix, VB1-10350-210) was used as a positive control to ensure good RNA quality. Samples were run using a 16-color Life Technologies Attune Nxt flow cytometer and data was analyzed using FlowJo software.

RESULTS

Validation of Inducible OPC Reporter Mouse Line

In order to selectively label oligodendrocyte progenitor cells (OPCs) in the adult mouse brain with as little off-target labeling as possible, we utilized a PDGFRα-Cre^{ER}; R26-EYFP mouse line[6]. Animals were injected with tamoxifen at 6 weeks of age to avoid labeling the pool of OPCs that differentiate into oligodendrocytes during developmental myelination[28]. Two tamoxifen injections were sufficient to label the majority (93.56% ± 1.98) of OPCs in the brain (Supplemental Fig. 1A, C). Immunohistochemistry revealed that yellow fluorescent protein positive cells (YFP+) following 2 tamoxifen injections were composed of OPCs (81.5%; PDGFRα+/Olig2+), mature oligodendrocytes (10.9%, PDGFRα-/Olig2+) or other cell types not belonging to the canonical oligolineage (7.6%, PDGFRα-/Olig2- or PDGFRα+/Olig2-), presumably endothelial cells, as they are also known to express PDGFRα (Supplemental Fig. 1B,D)[29].

Isolation and Sequencing of YFP+ Cells

Whole brains, including the cerebellum but excluding the spinal cord, were collected from adult PDGFRα-Cre^{ER}; R26-EYFP mice and processed into a single-cell suspension for FACS. Four to five brains were pooled for each sample, and male and female brains were processed separately to allow for analysis of potential sex differences in YFP+ cells (Supplemental Fig. 2A). YFP+ cells were selected by gating on live cells while excluding immune (CD45+) and red blood cells (TER119+), thus ensuring that the population of YFP+ cells collected were viable and highly enriched (Supplemental Fig. 2B). YFP+ cells were barcoded and prepared for single-cell sequencing using Next GEM reagents and Chromium microfluidics supplied by 10x Genomics. Cell sorting and sequencing was performed three independent times for a total of 6 independently sequenced samples. Unbiased clustering of each independent run revealed overlap between distinct sequencing runs and no clustering of cells driven by sequencing run alone (Supplemental Fig. 3A). For all future analysis, all sequencing runs were combined to form one large dataset.

Profiling the Molecular Signature of OPCs in the Adult Brain

Unbiased clustering of sequenced cells using the Seurat package[22,23] revealed that cells sorted from PDGFRα-Cre^{ER}; R26-EYFP brains clustered into 8 distinct populations (Fig. 1A). Mature oligodendrocytes comprise one cluster, having potentially differentiated following initial tamoxifen labeling of PDGFRα expressing progenitor cells. Also captured in the sequencing were three cell-types outside the oligolineage that are known to either express PDGFRα or come from PDGFRα expressing precursors, including fibroblasts, endothelial cells, and 2 populations of pericytes[29-32]. These clusters were identified by expression of known cell type markers such as *Igfbp6* and *Fn1* (fibroblasts), *Tek*, *Pecam1*, and *Kdr* (endothelial cells), as well as *Rgs5*, *Pdgfrb*, and *Des* (pericytes)[33-36]. The remaining 3 clusters of cells (OPC1, OPC2, and OPC3) expressed at least 2 of the 5 canonical OPC markers *Ptprz*, *PDGFRα*, *Olig1*, *Olig2*, and *Cspg4* (Fig. 1B). Importantly, each OPC cluster of cells expressed a unique transcriptional signature distinct from the gene expression in every other cluster (Fig. 1C).

In order to further investigate how these clusters of OPCs are distinct from one another, we identified a significantly upregulated gene from each cluster that offered potential indications of distinct functions of these subpopulations (Fig. 1D). OPC1 expressed high levels of *Clusterin*, a secreted glycoprotein that can play either pro-apoptotic or anti-apoptotic roles, depending on the splice variant that a cell expresses[37-39]. OPC2 expressed high levels of *Lumican*, an extracellular matrix protein known to bind collagen and play an important role in tissue healing[40-42]. OPC3 shows significant upregulation of the G-protein coupled receptor *Gpr17*, the only currently known marker of molecular diversity in OPCs, when compared to all other cell types sequenced (Fig. 1D)[43,44].

Lastly, in order to gain insight into how these subpopulations of OPCs potentially differ at the functional level, we analyzed GO terms that were significantly upregulated in each OPC cluster and were not shared with either of the other OPC clusters (Fig. 1E). OPC1 showed unique upregulation in genes involved in ATP metabolic processes, cellular respiration, and oxidative phosphorylation, including *Chchd10*, *Mdh1*, and *Uqcrq*. Genes related to extracellular matrix organization, cytokine-mediated signaling pathways, and

regulation of cell-cell adhesion were significantly upregulated in OPC2, and included genes such as *Mfap4*, *Ifitm2*, and *Lgals1*. Lastly, OPC3 show unique upregulation in genes involved in the positive regulation of neuron differentiation, synapse organization, and cerebral cortex cell migration, including *Stmn2*, *Pfn2*, and *Dcx* (Supplemental Table 1).

In sum, our single sequencing data reveal three unique subpopulations of OPCs that reside in the adult brain under homeostatic conditions and are suggestive of functional diversity based on unique gene expression profile.

Sex Differences in OPCs

Since sex differences have been implicated in multiple types of glia including microglia and astrocytes, we investigated whether OPCs isolated from male or female mice exhibited significant transcriptional differences[45,46]. Interestingly, both males and female cells were found in all 8 clusters, and the number of significantly different genes between male and female cells in each cluster fell within the range of statistical noise (data not shown). However, each cluster of OPCs did not have an equal distribution of cells from males and females, with males exhibiting a higher frequency of cells in OPC1 and females exhibiting a higher frequency of cells in OPC3. A relatively equivalent frequency was found in OPC2 (Supplemental Fig. 3C). While this data indicates that no sex-specific OPC signature found in the adult brain, the proportions of OPC subpopulations may be sexually dimorphic.

In Vivo Validation of OPC Subpopulations

Since gene expression can be altered by tissue processing before sequencing[47], we validated the expression of each OPC cluster marker using RNAscope in adult mouse brain. OPCs were defined by the co-expression of two canonical OPC transcripts encoding for cell surface markers (*Pdgfra* or *Cspg4*) and oligolineage transcription factors (*Olig1* or *Olig2*). Using a Cell Profiler pipeline to unbiasedly quantify RNA puncta expression per cell[26], we subsequently quantified expression of each OPC cluster gene. OPCs in both gray and white matter express a range of both *Clusterin* and *Gpr17* transcripts, with a population of cells expressing little to no RNA for these markers, a

population of cells showing medium expression, and a smaller population of cells expressing very high levels of these transcripts (Fig 2A, C). *Lumican*, the marker for OPC2, showed much lower expression in the brain, although we still observed some OPCs expressing low levels of *Lumican*, and many OPCs expressing no observable levels of *Lumican* (Fig 2B). We were therefore able to detect and validate, using the novel selected cluster markers and canonical OPC genes, each cluster of OPCs *in vivo*.

Expression of Canonical Markers in OPC Clusters

While single-cell sequencing provides gene expression data on an individual cell basis, its relatively shallow depth of sequencing can result in little to no detected expression of genes with known low expression[48,49]. In order to confirm that the 3 identified clusters of OPCs express canonical OPC markers using a more sensitive method of gene detection, we individually sorted each cluster of OPCs based on expression of cell surface proteins. OPC1 was identified by expression of Aquaporin1 (Supplemental Fig 4A), OPC2 was identified by expression of Decorin (Supplemental Fig. 4B), and OPC3 was identified by expression of Neurexin1 (Supplemental Fig. 4C). Each cluster of OPCs was sorted by FACS based on their co-expression of YFP and Aquaporin1 (for OPC1), Decorin (for OPC2), and Neurexin1 (for OPC3) (Supplemental Fig. 4D). Expression of *Olig1*, *Olig2, Pdgfra*, and *Cspg4* was then determined by qPCR. While each cluster demonstrated expression of at least 2 canonical OPC markers, each cluster demonstrated a unique combination of each of these genes (Fig. 3A). For example, OPC1 expresses *Olig1*, *Olig2*, and *Pdgfra* with relatively low expression of *Cspg4*, OPC3 expresses both *Pdgfra* and *Cspg4* with relatively low expression of *Olig1* and *Olig2*, and OPC2 expresses all 4 canonical markers. Our results offer additional validation of canonical OPC marker expression in the 3 clusters of adult OPCs identified by single-cell sequencing.

***Clusterin* and *Gpr17* are exclusively expressed in OPC1 and OPC3 subsets**

While both RNAscope and RT-qPCR of canonical OPC markers within each cluster have demonstrated that these clusters of OPCs are expressed within the brain and belong to the oligolineage, neither of these techniques have demonstrated that these markers characterize clusters that are unique from one another. Using PrimeFlow, a technique

that allows for the combination of cellular-resolution RNA detection with the multiplexing capabilities of flow cytometry, we demonstrate that a subset of *Olig2* expressing cells express *Clusterin* (OPC1), and a mutually exclusive population expresses *Gpr17* (OPC3), with very few OPCs expressing detectable levels of both cluster markers (Fig 3. B,C). While this does not rule out the possibility that an individual OPC might express genes enriched in different clusters at different times, it does demonstrate that, at any given point, genetic markers of these 2 clusters of OPCs largely do not overlap.

Discussion

With the development of novel tools that allow for the analysis of tissue at single-cell resolution, interest has surged in outlining how cell-types that express the same canonical cell type markers may represent more diverse subpopulations than previously thought[50-54]. Here, we demonstrate that OPCs from the adult brain cluster into three distinct subpopulations characterized by a transcriptional signature and Gene Ontology profile.

A small number of studies have investigated the transcriptional profiles of OPCs present during development and have described relatively little transcriptional diversity. Marques and colleagues transcriptionally profiled oligolineage cells from both juvenile and adult brains and, while mature oligodendrocytes clustered into seven subpopulations, their data indicated one population of progenitor cells[54]. However, their population of sequenced OPCs was relatively small (approximately 300 cells) and the majority of their OPCs came from juvenile animals[54]. A more recent study from the same group characterized the transcriptional profiles of OPCs from E13.5, E17.5, and P7 mice and found three clusters of OPCs that shared similar transcriptional signatures, but clustered by the age of the cells, and one cluster of cycling OPCs[32]. From this data, they concluded that, during development, the three known waves of developmental OPCs converge into a transcriptionally homogenous group of OPCs by P7. Importantly, this sequencing dataset only profiles prenatal and early postnatal OPCs, a time window in which OPCs are preparing to generate a large population of mature oligodendrocytes to support the developmental myelination that occurs during early postnatal timepoints[28]. Therefore, it is likely that OPCs during this early stage of development may represent a relatively homogenous population of progenitors destined to give rise to myelinating glia[28]. However, following developmental myelination, oligodendrocytes represent a relatively stable population that require minimal replacement, yet OPCs continue to represent approximately 5% of cells in the adult brain and tile every brain region[2,55]. It is therefore reasonable to hypothesize that as the CNS matures, and no longer requires the production of large numbers of mature oligodendrocytes, OPCs may develop diverse transcriptional repertoires, as demonstrated here, to perform alternative functions throughout adulthood. Indeed, recent data from Spitzer and colleagues demonstrated that

OPCs throughout the brain express a diverse array of electrophysiological properties and ion channels and that these characteristics become more diverse with age[13]. Additionally, data obtained from zebrafish has demonstrated that OPCs can be categorized into two functionally distinct subpopulations that demonstrate different calcium dynamics[56]. Interestingly, one population of OPCs was found to rarely differentiate *in vivo*, although these cells maintained their differentiation capacity, indicating that the main functions of this population of OPCs is likely something other than serving as a progenitor pool for mature oligodendrocytes[56].

Our in-depth analysis of canonical OPC marker expression in each OPC cluster surprisingly indicated that both OPC1 and OPC3 expressed a unique subset of common OPC markers. While PDGFRα, CSPG4, Olig1, and Olig2 have historically all been thought to be expressed in the vast majority of OPCs[57], recent data from zebrafish indicates that approximately 80% of gray-matter OPCs and 30% of white matter OPCs express *Cspg4* transcripts[56]. This differential expression of canonical OPC markers may indicate that OPCs can express a unique array of OPC genes based on their function, and canonical OPC markers may not be as critical to OPC functioning as previously thought. This idea is supported by the recent description of the development and differentiation of a PDGFRα-independent subpopulation of OPCs[58].

It is also important to note that both sequencing studies previously mentioned utilized different mouse lines to identify OPCs than the PDGFRα-Cre^{ER}; R26-EYFP used in this study, which may have also contributed to the difference between our dataset and the previous observations of a homogenous population of OPCs. Excitingly, recent sequencing data from human Alzheimer's disease patients and healthy controls demonstrated that healthy controls have three subpopulations of OPCs, and that one of these populations expressed high levels of *Clusterin*, one of the genes we identified as significantly upregulated in OPC1[59]. Additionally, single-cell sequencing data from human patients at fetal, adolescent, and adult timepoints reveal multiple transcriptionally distinct populations of oligo-lineage cells that largely clustered based on the age of the patient[60]. The addition of our study to the previously published datasets, detailing the transcriptional

profile of developmental OPCs will provide the field with a better understanding of how OPCs might change as the brain matures. Indeed, our works highlights how the function of OPCs might shift as development ends and the brain enters adulthood.

Many of the differentially expressed genes and related biological processes found in each OPC cluster complement emerging literature that indicates non-canonical roles for OPCs during homeostasis, and a more active role of this cell type in multiple diseases. For example, OPC1 expresses high levels of *Clusterin*, a gene known to be upregulated in both Alzheimer's disease and multiple sclerosis (MS)[61,62]. OPCs have recently been shown to potentially play an active role in the pathology of MS and have been implicated in the progression of Alzheimer's disease[17,20,63]. Given these associations with Alzheimer's disease and MS, and the known role of clusterin in multiple CNS pathologies, interrogating the functions of this cluster of OPCs may be particularly important in revealing novel ways OPCs help maintain homeostasis and how they subsequently may be playing an active role in contributing to or protecting against CNS pathology[63-66].

OPC2 shows particular enrichment of *Lumican*, an important extracellular matrix component and potent modulator of multiple signaling pathways[41,67]. In addition to *Lumican*, multiple other proteins involved in extracellular matrix organization, a role already attributed to OPCs, are particularly enriched in this cluster[68-70]. Intriguingly, *Lumican* is known to be involved in the recruitment of immune cells and the regulation of cellular infiltration of tissue[71-74]. This cluster showed significant upregulation of genes related to cytokine mediated signaling, consistent with recent papers indicating that OPCs may be playing an active role in regulating the immune system, interrogating the function and transcriptional signature of this cluster of OPCs may further elucidate how OPCs may be interacting with the immune system and modulating the CNS environment to affect neuronal behavior and function[16,17,20,63].

OPC3 shows significant upregulation of the G-protein coupled receptor *Gpr17* (Fig. 1D). Importantly, *Gpr17* is the only documented marker of molecular diversity in OPCs described to date and is only found in one cluster of OPCs in our dataset[43,44]. This cluster

shows unique upregulation of genes related to neuronal differentiation and synapse organization (Fig. 1E). These processes are particularly intriguing given that OPCs are the only known glial cell to form canonical synapses with neurons, and have recently been shown to be critical in regulating circuit formation during development[12,75]. Birey and colleagues demonstrated that ablating OPCs significantly altered neuronal function and resulted in depressive and anxiety-like behavior[14]. It still remains to be seen if this effect of OPC loss on neuronal function is mediated through another cell type. Yet those studies, coupled with the sequencing data described here, makes investigation of this subpopulation of OPCs crucial in understanding how OPCs are directly influencing neuronal health, circuit functioning and formation, and overall behavioral outcomes.

While we describe the transcriptional profile of OPCs during homeostasis, it is important to note that understanding the role of OPCs in the healthy brain will provide a necessary foundation for examining any protective or detrimental novel functions in desease pathology. Previous work has demonstrated that OPCs exhibit significant transcriptional heterogeneity and disease-associated signatures in models of multiple sclerosis and cerebral ischemia, and showed significant transcriptional changes in human Alzheimer's disease patients[18,59,76].

We believe that the work presented here provides a critical foundation and basis for the investigation of non-canonical roles of OPCs This dataset will not only assist the field in discovering novel roles for OPCs in both health and disease, but can also offer potential mechanistic explanations for intriguing phenotypes observed in OPC deletion paradigms[14-17].

Bibliography

1 Raff, M. C., Miller, R. H. & Noble, M. A Glial Progenitor-Cell That Develops Invitro into an Astrocyte or an Oligodendrocyte Depending on Culture-Medium. *Nature* **303**, 390-396, doi:DOI 10.1038/303390a0 (1983).

2 Dawson, M. R., Polito, A., Levine, J. M. & Reynolds, R. NG2-expressing glial progenitor cells: an abundant and widespread population of cycling cells in the adult rat CNS. *Mol Cell Neurosci* **24**, 476-488 (2003).

3 Geha, S. *et al.* NG2+/Olig2+ cells are the major cycle-related cell population of the adult human normal brain. *Brain Pathol* **20**, 399-411, doi:10.1111/j.1750-3639.2009.00295.x (2010).

4 Simon, C., Gotz, M. & Dimou, L. Progenitors in the adult cerebral cortex: cell cycle properties and regulation by physiological stimuli and injury. *Glia* **59**, 869-881, doi:10.1002/glia.21156 (2011).

5 Hughes, E. G., Kang, S. H., Fukaya, M. & Bergles, D. E. Oligodendrocyte progenitors balance growth with self-repulsion to achieve homeostasis in the adult brain. *Nature neuroscience* **16**, 668-676, doi:10.1038/nn.3390 (2013).

6 Kang, S. H., Fukaya, M., Yang, J. K., Rothstein, J. D. & Bergles, D. E. NG2+ CNS glial progenitors remain committed to the oligodendrocyte lineage in postnatal life and following neurodegeneration. *Neuron* **68**, 668-681, doi:10.1016/j.neuron.2010.09.009 (2010).

7 Yeung, M. S. *et al.* Dynamics of oligodendrocyte generation and myelination in the human brain. *Cell* **159**, 766-774, doi:10.1016/j.cell.2014.10.011 (2014).

8 Tripathi, R. B. *et al.* Remarkable Stability of Myelinating Oligodendrocytes in Mice. *Cell Rep* **21**, 316-323, doi:10.1016/j.celrep.2017.09.050 (2017).

9 Gibson, E. M. *et al.* Neuronal Activity Promotes Oligodendrogenesis and Adaptive Myelination in the Mammalian Brain. *Science* **344** (2014).

10 Mackenzie, S. *et al.* Depression and suicide ideation among students accessing campus health care. *The American journal of orthopsychiatry* **81**, 101-107, doi:10.1111/j.1939-0025.2010.01077.x (2011).

11 Dimou, L. & Simons, M. Diversity of oligodendrocytes and their progenitors. *Current opinion in neurobiology* **47**, 73-79, doi:10.1016/j.conb.2017.09.015 (2017).

12 Orduz, D. *et al.* Developmental cell death regulates lineage-related interneuron-oligodendroglia functional clusters and oligodendrocyte homeostasis. *Nat Commun* **10**, 4249, doi:10.1038/s41467-019-11904-4 (2019).

13 Spitzer, S. O. *et al.* Oligodendrocyte Progenitor Cells Become Regionally Diverse and Heterogeneous with Age. *Neuron*, doi:10.1016/j.neuron.2018.12.020 (2019).

14 Birey, F. *et al.* Genetic and Stress-Induced Loss of NG2 Glia Triggers Emergence of Depressive-like Behaviors through Reduced Secretion of FGF2. *Neuron* **88**, 941-956, doi:10.1016/j.neuron.2015.10.046 (2015).

15 Djogo, T. *et al.* Adult NG2-Glia Are Required for Median Eminence-Mediated Leptin Sensing and Body Weight Control. *Cell Metab* **23**, 797-810, doi:10.1016/j.cmet.2016.04.013 (2016).

16 Nakano, M. *et al.* NG2 glial cells regulate neuroimmunological responses to maintain neuronal function and survival. *Sci Rep* **7**, 42041, doi:10.1038/srep42041 (2017).
17 Kang, Z. *et al.* Act1 mediates IL-17-induced EAE pathogenesis selectively in NG2+ glial cells. *Nature neuroscience* **16**, 1401-1408, doi:10.1038/nn.3505 (2013).
18 Falcao, A. M. *et al.* Disease-specific oligodendrocyte lineage cells arise in multiple sclerosis. *Nat Med*, doi:10.1038/s41591-018-0236-y (2018).
19 Kirby, L. *et al.* Oligodendrocyte precursor cells present antigen and are cytotoxic targets in inflammatory demyelination. *Nature Communications* **10**, 3887, doi:10.1038/s41467-019-11638-3 (2019).
20 Fernández-Castañeda, A. *et al.* The active contribution of OPCs to neuroinflammation is mediated by LRP1. *Acta Neuropathologica*, doi:10.1007/s00401-019-02073-1 (2019).
21 Baxi, E. G. *et al.* A selective thyroid hormone beta receptor agonist enhances human and rodent oligodendrocyte differentiation. *Glia* **62**, 1513-1529, doi:10.1002/glia.22697 (2014).
22 Butler, A., Hoffman, P., Smibert, P., Papalexi, E. & Satija, R. Integrating single-cell transcriptomic data across different conditions, technologies, and species. *Nat Biotechnol* **36**, 411-420, doi:10.1038/nbt.4096 (2018).
23 Stuart, T. *et al.* Comprehensive Integration of Single-Cell Data. *Cell* **177**, 1888-1902 e1821, doi:10.1016/j.cell.2019.05.031 (2019).
24 Buettner, F. *et al.* Computational analysis of cell-to-cell heterogeneity in single-cell RNA-sequencing data reveals hidden subpopulations of cells. *Nat Biotechnol* **33**, 155-160, doi:10.1038/nbt.3102 (2015).
25 Yu, G. C., Wang, L. G., Han, Y. Y. & He, Q. Y. clusterProfiler: an R Package for Comparing Biological Themes Among Gene Clusters. *Omics-a Journal of Integrative Biology* **16**, 284-287, doi:10.1089/omi.2011.0118 (2012).
26 Erben, L., He, M.-X., Laeremans, A., Park, E. & Buonanno, A. A Novel Ultrasensitive In Situ Hybridization Approach to Detect Short Sequences and Splice Variants with Cellular Resolution. *Molecular neurobiology* **55**, 6169-6181, doi:10.1007/s12035-017-0834-6 (2018).
27 Hrvatin, S. *et al.* Single-cell analysis of experience-dependent transcriptomic states in the mouse visual cortex. *Nature neuroscience* **21**, 120-129, doi:10.1038/s41593-017-0029-5 (2018).
28 Semple, B. D., Blomgren, K., Gimlin, K., Ferriero, D. M. & Noble-Haeusslein, L. J. Brain development in rodents and humans: Identifying benchmarks of maturation and vulnerability to injury across species. *Prog Neurobiol* **106-107**, 1-16, doi:10.1016/j.pneurobio.2013.04.001 (2013).
29 Aghajanian, H. *et al.* Pdgfrα functions in endothelial-derived cells to regulate neural crest cells and the development of the great arteries. *Disease Models & Mechanisms* **10**, 1101-1108 (2017).
30 Li, R. *et al.* Pdgfra marks a cellular lineage with distinct contributions to myofibroblasts in lung maturation and injury response. *eLife* **7**, e36865, doi:10.7554/eLife.36865 (2018).

31 Endale, M. *et al.* Temporal, spatial, and phenotypical changes of PDGFRα expressing fibroblasts during late lung development. *Developmental biology* **425**, 161-175, doi:10.1016/j.ydbio.2017.03.020 (2017).

32 Marques, S. *et al.* Transcriptional Convergence of Oligodendrocyte Lineage Progenitors during Development. *Developmental Cell* (2018).

33 Witmer, A. N., van Blijswijk, B. C., van Noorden, C. J. F., Vrensen, G. F. J. M. & Schlingemann, R. O. In vivo angiogenic phenotype of endothelial cells and pericytes induced by vascular endothelial growth factor-A. *The journal of histochemistry and cytochemistry : official journal of the Histochemistry Society* **52**, 39-52, doi:10.1177/002215540405200105 (2004).

34 Xiao, W. *et al.* Ozone oil promotes wound healing by increasing the migration of fibroblasts via PI3K/Akt/mTOR signaling pathway. *Biosci Rep* **37**, BSR20170658, doi:10.1042/BSR20170658 (2017).

35 Bondjers, C. *et al.* Transcription profiling of platelet-derived growth factor-B-deficient mouse embryos identifies RGS5 as a novel marker for pericytes and vascular smooth muscle cells. *The American journal of pathology* **162**, 721-729, doi:10.1016/S0002-9440(10)63868-0 (2003).

36 Smyth, L. C. D. *et al.* Markers for human brain pericytes and smooth muscle cells. *J Chem Neuroanat* **92**, 48-60, doi:10.1016/j.jchemneu.2018.06.001 (2018).

37 Jordan-Starck, T. C. *et al.* Mouse apolipoprotein J: characterization of a gene implicated in atherosclerosis. *Journal of lipid research* **35**, 194-210 (1994).

38 Kim, N. & Choi, W. S. Proapoptotic role of nuclear clusterin in brain. *Anat Cell Biol* **44**, 169-175, doi:10.5115/acb.2011.44.3.169 (2011).

39 Zhang, H. *et al.* Clusterin inhibits apoptosis by interacting with activated Bax. *Nature cell biology* **7**, 909-915, doi:10.1038/ncb1291 (2005).

40 Svensson, L., Närlid, I. & Oldberg, A. Fibromodulin and lumican bind to the same region on collagen type I fibrils. *Febs Lett* **470**, 178-182, doi:10.1016/s0014-5793(00)01314-4 (2000).

41 Karamanou, K., Perrot, G., Maquart, F.-X. & Brézillon, S. Lumican as a multivalent effector in wound healing. *Advanced drug delivery reviews* **129**, 344-351, doi:10.1016/j.addr.2018.02.011 (2018).

42 Yeh, J. T. *et al.* Impaired skin wound healing in lumican-null mice. *Br J Dermatol* **163**, 1174-1180, doi:10.1111/j.1365-2133.2010.10008.x (2010).

43 Fumagalli, M. *et al.* Phenotypic changes, signaling pathway, and functional correlates of GPR17-expressing neural precursor cells during oligodendrocyte differentiation. *J Biol Chem* **286**, 10593-10604, doi:10.1074/jbc.M110.162867 (2011).

44 Vigano, F. *et al.* GPR17 expressing NG2-Glia: Oligodendrocyte progenitors serving as a reserve pool after injury. *Glia* **64**, 287-299, doi:10.1002/glia.22929 (2016).

45 Villa, A. *et al.* Sex-Specific Features of Microglia from Adult Mice. *Cell reports* **23**, 3501-3511, doi:10.1016/j.celrep.2018.05.048 (2018).

46 Santos-Galindo, M., Acaz-Fonseca, E., Bellini, M. J. & Garcia-Segura, L. M. Sex differences in the inflammatory response of primary astrocytes to lipopolysaccharide. *Biology of sex differences* **2**, 7, doi:10.1186/2042-6410-2-7 (2011).

47 van den Brink, S. C. *et al.* Single-cell sequencing reveals dissociation-induced gene expression in tissue subpopulations. *Nature methods* **14**, 935-936, doi:10.1038/nmeth.4437 (2017).
48 Marinov, G. K. *et al.* From single-cell to cell-pool transcriptomes: stochasticity in gene expression and RNA splicing. *Genome research* **24**, 496-510, doi:10.1101/gr.161034.113 (2014).
49 Grün, D., Kester, L. & van Oudenaarden, A. Validation of noise models for single-cell transcriptomics. *Nature methods* **11**, 637-640, doi:10.1038/nmeth.2930 (2014).
50 Hammond, T. R. *et al.* Single-Cell RNA Sequencing of Microglia throughout the Mouse Lifespan and in the Injured Brain Reveals Complex Cell-State Changes. *Immunity* **50**, 253-271.e256, doi:10.1016/j.immuni.2018.11.004 (2019).
51 Masuda, T. *et al.* Spatial and temporal heterogeneity of mouse and human microglia at single-cell resolution. *Nature* **566**, 388-392, doi:10.1038/s41586-019-0924-x (2019).
52 Xin, W. & Bonci, A. Functional Astrocyte Heterogeneity and Implications for Their Role in Shaping Neurotransmission. *Frontiers in cellular neuroscience* **12**, 141-141, doi:10.3389/fncel.2018.00141 (2018).
53 John Lin, C.-C. *et al.* Identification of diverse astrocyte populations and their malignant analogs. *Nature neuroscience* **20**, 396-405, doi:10.1038/nn.4493 (2017).
54 Marques, S. *et al.* Oligodendrocyte heterogeneity in the mouse juvenile and adult central nervous system. *Science* **352**, 1326-1329, doi:10.1126/science.aaf6463 (2016).
55 Mackie, M., Hughes, D. I., Maxwell, D. J., Tillakaratne, N. J. & Todd, A. J. Distribution and colocalisation of glutamate decarboxylase isoforms in the rat spinal cord. *Neuroscience* **119**, 461-472 (2003).
56 Marisca, R. *et al.* Functionally distinct subgroups of oligodendrocyte precursor cells integrate neural activity and execute myelin formation. *Nature neuroscience*, doi:10.1038/s41593-019-0581-2 (2020).
57 Foerster, S., Hill, M. F. E. & Franklin, R. J. M. Diversity in the oligodendrocyte lineage: Plasticity or heterogeneity? *Glia* **67**, 1797-1805, doi:10.1002/glia.23607 (2019).
58 Zheng, K. *et al.* Molecular and Genetic Evidence for the PDGFRα-Independent Population of Oligodendrocyte Progenitor Cells in the Developing Mouse Brain. *The Journal of neuroscience : the official journal of the Society for Neuroscience* **38**, 9505-9513, doi:10.1523/JNEUROSCI.1510-18.2018 (2018).
59 Grubman, A. *et al.* A single-cell atlas of entorhinal cortex from individuals with Alzheimer's disease reveals cell-type-specific gene expression regulation. *Nature neuroscience* **22**, 2087-2097, doi:10.1038/s41593-019-0539-4 (2019).
60 Perlman, K. *et al.* Developmental trajectory of oligodendrocyte progenitor cells in the human brain revealed by single cell RNA sequencing. *Glia* **n/a**, doi:10.1002/glia.23777 (2020).
61 Loveless, S. *et al.* Tissue microarray methodology identifies complement pathway activation and dysregulation in progressive multiple sclerosis. *Brain Pathology* **28**, 507-520, doi:10.1111/bpa.12546 (2018).

62 Miners, J. S., Clarke, P. & Love, S. Clusterin levels are increased in Alzheimer's disease and influence the regional distribution of Aβ. *Brain pathology (Zurich, Switzerland)* **27**, 305-313, doi:10.1111/bpa.12392 (2017).

63 Zhang, P. *et al.* Senolytic therapy alleviates Aβ-associated oligodendrocyte progenitor cell senescence and cognitive deficits in an Alzheimer's disease model. *Nature neuroscience* **22**, 719-728, doi:10.1038/s41593-019-0372-9 (2019).

64 Green, A. J. *et al.* Clemastine fumarate as a remyelinating therapy for multiple sclerosis (ReBUILD): a randomised, controlled, double-blind, crossover trial. *Lancet (London, England)* **390**, 2481-2489, doi:10.1016/S0140-6736(17)32346-2 (2017).

65 Cadavid, D. *et al.* Safety and efficacy of opicinumab in patients with relapsing multiple sclerosis (SYNERGY): a randomised, placebo-controlled, phase 2 trial. *The Lancet. Neurology* **18**, 845-856, doi:10.1016/S1474-4422(19)30137-1 (2019).

66 Schwartzbach, C. J. *et al.* Lesion remyelinating activity of GSK239512 versus placebo in patients with relapsing-remitting multiple sclerosis: a randomised, single-blind, phase II study. *Journal of neurology* **264**, 304-315, doi:10.1007/s00415-016-8341-7 (2017).

67 Nikitovic, D., Katonis, P., Tsatsakis, A., Karamanos, N. K. & Tzanakakis, G. N. Lumican, a small leucine-rich proteoglycan. *IUBMB Life* **60**, 818-823, doi:10.1002/iub.131 (2008).

68 Garwood, J. *et al.* The extracellular matrix glycoprotein Tenascin-C is expressed by oligodendrocyte precursor cells and required for the regulation of maturation rate, survival and responsiveness to platelet-derived growth factor. *European Journal of Neuroscience* **20**, 2524-2540, doi:10.1111/j.1460-9568.2004.03727.x (2004).

69 Jones, L. L. & Tuszynski, M. H. Spinal cord injury elicits expression of keratan sulfate proteoglycans by macrophages, reactive microglia, and oligodendrocyte progenitors. *J Neurosci* **22**, 4611-4624, doi:20026464 (2002).

70 Tang, X., Davies, J. E. & Davies, S. J. A. Changes in distribution, cell associations, and protein expression levels of NG2, neurocan, phosphacan, brevican, versican V2, and tenascin-C during acute to chronic maturation of spinal cord scar tissue. *Journal of Neuroscience Research* **71**, 427-444, doi:10.1002/jnr.10523 (2003).

71 Lohr, K. *et al.* Extracellular matrix protein lumican regulates inflammation in a mouse model of colitis. *Inflammatory bowel diseases* **18**, 143-151, doi:10.1002/ibd.21713 (2012).

72 Tomlin, H. & Piccinini, A. M. A complex interplay between the extracellular matrix and the innate immune response to microbial pathogens. *Immunology* **155**, 186-201, doi:10.1111/imm.12972 (2018).

73 Coulson-Thomas, V. J. *et al.* Lumican expression, localization and antitumor activity in prostate cancer. *Experimental cell research* **319**, 967-981, doi:10.1016/j.yexcr.2013.01.023 (2013).

74 Wu, F. *et al.* A novel role of the lumican core protein in bacterial lipopolysaccharide-induced innate immune response. *The Journal of biological chemistry* **282**, 26409-26417, doi:10.1074/jbc.M702402200 (2007).

75 Bergles, D. E., Roberts, J. D., Somogyi, P. & Jahr, C. E. Glutamatergic synapses on oligodendrocyte precursor cells in the hippocampus. *Nature* **405**, 187-191, doi:10.1038/35012083 (2000).

76 Valny, M. *et al.* A single-cell analysis reveals multiple roles of oligodendroglial lineage cells during post-ischemic regeneration. *Glia* **66**, 1068-1081, doi:10.1002/glia.23301 (2018).

FIGURE LEGENDS

Figure 1: Adult OPCs cluster in three distinct subpopulations. (A) tSNE plot of all sequenced cells isolated from PDGFRα-Cre^{ER} reporter brains. Clusters were labeled with cell-type classifications based on expression of common cell-type markers. N=3 independent experiments, n=6 samples. (B) Violin plots depicting expression of common OPC markers in each cluster. Each dot represents a cell. Expression value is plotted on the y-axis. (C) Heatmap depicting the scaled and log-normalized expression values of the top 10 most highly enriched genes in each cluster. (D) Cell-specific expression of markers used for cluster validation including *clusterin* (OPC1), *lumican* (OPC2), and *Gpr17* (OPC3) overlaid on tSNE map. (E) Significant GO terms uniquely upregulated in one OPC cluster compared to the other two OPC clusters. PC=Pericytes.

Figure 2: In vivo OPC expression of cluster markers clusterin, lumican, and GPR17. (A) RNAscope expression of *Pdgfrα* (red), *Olig1* (green), *Clu* (white), and Hoechst (blue). Quantification of the number of *Clu* transcripts in individual OPCs. Data plotted as a histogram of *Clu* expression in OPCs with a bin width of 10 transcripts. N=2 individual experiments, n=4 samples, with a total of 205 OPCs quantified. (B) RNAscope expression of *Pdgfrα* (red), *Olig2* (green), *Lum* (white), and DAPI (blue). Quantification of the number of *Lum* transcripts in individual OPCs. Data plotted as a histogram of *Lum* expression in OPCs with a bin width of 2 transcripts. N=3 individual experiments, n=4 samples, with a total of 205 OPCs quantified. (C) RNAscope expression of *Pdgfrα* (red), *Olig2* (green), *Gpr17* (white), and Hoechst (blue). Quantification of the *Gpr17* expression in OPCs with a bin width of 5 transcripts. N=3 individual experiments, n=4 samples, with a total of 247 OPCs quantified. In all RNAscope experiments, OPCs were identified as cells co-expressing an OPC surface marker (*Pdgfrα* or *Cspg4*) and an oligolineage transcription factor (*Olig1* or *Olig2*). Each sample includes quantification of marker expression from the cortex, hippocampus, corpus callosum, and cerebellum. Scale bar = 10μM

Figure 3: OPC clusters express multiple canonical OPC markers, but do not express markers of multiple clusters. (A) qPCR relative quantification of canonical OPC markers *Olig1*, *Olig2*, *Pdgfrα*, and *Cspg4* in OPC1 (YFP+/AQP1+), OPC2 (YFP+/DCN+), OPC3 (YFP+/NRXN1+), and all YFP+ cells. Values plotted are the $2^{-\Delta\Delta Cq}$ relative to the average ΔCq in all YFP+ cells. N=4 independent experiments, n=4 samples per group. (B) Representative PrimeFlow gating of brain cells stained for CD45 protein and *Clu*, *Gpr17*, *Pdgfrα*, and *Olig2* RNA. (C) Quantification of Live/CD45-/Olig2+ cells that express *Clu* alone, *Gpr17* alone, or both *Clusterin* and *Gpr17*. N=2 individual experiments, n=9 samples. Analyzed using one-way repeated measures ANOVA. ****p<0.0001, *p<0.05. Error bars represent SEM.

Supplemental Figure 1: Validation of PDGFRα-Cre^{ER}; R26-EYFP reporter mouse. (A) Timeline of tamoxifen injections and tissue harvest used to validate YFP expression in OPCs and titrate optimal tamoxifen dosing paradigm. (B) Immunofluorescence of PDGFRα (red), Olig2 (blue), and YFP (green) in PDGFRα-Cre^{ER}; R26-eYFP mice receiving no tamoxifen injections (- Tamoxifen) or 2 tamoxifen injections (+Tamoxifen). Arrows represent OPCs expressing YFP and arrowheads represent OPCs lacking YFP expression. Scale bar = 30μM. (C) Percentage of OPCs (PDGFRα+/Olig2+) that also express YFP following 0, 1, 2, or 3 tamoxifen injections. N=3 independent experiments, n=2-3 per group. Error bars represent SEM. (D) Proportion of YFP+ cells identified as OPCs (PDGFRα+/Olig2+), Oligodendrocytes (OLG, PDGFRα-/Olig2+), or neither of these cell types (Other, PDGFRα+/Olig2- or PDGFRα-/Olig2-) following 2 tamoxifen injections. N=2 independent experiments, n=3 samples. Data quantified in (C) and (D) include images from the prefrontal cortex, hippocampus, and corpus callosum.

Supplemental Figure 2: Isolation of YFP+ cells from PDGFRα-creERT2 x YFP brains for sequencing. (A) Experimental strategy used for the isolation and single-cell sequencing of cells analyzed in Figure 1. (B) Gating strategy for YFP+ cell sorting following Live/Scatter/Singlet gating.

Supplemental Figure 3: (A) tSNE map depicting cell clusters colored by sequencing run. (B) tSNE map depicting cell clusters colored by sequencing sex. (C) Percent of male and female cells that fall within each cluster. Each bar represents the percentage of all male (blue) or female (red) cells sequenced.

Supplemental Figure 4: Isolation of Specific OPC clusters. Expression of genes used to sort out individual OPC clusters including *Aquaporin1* (A), *Decorin* (B), and *Neurexin 1* (C) overlaid on tSNE map. (D) Gating strategy used to isolate OPC1 (YFP+/AQP1+), OPC2 (YFP+/DCN+), and OPC3 (YFP+/NRXN1+) clusters from brains of PDGFRα-creERT2 x YFP mice.

Supplemental Table 1: Most highly enriched genes in each OPC cluster. Top 60 most highly enriched genes in each OPC cluster. Log-fold change is calculated based on comparison to all sequenced cells.

Figure 1

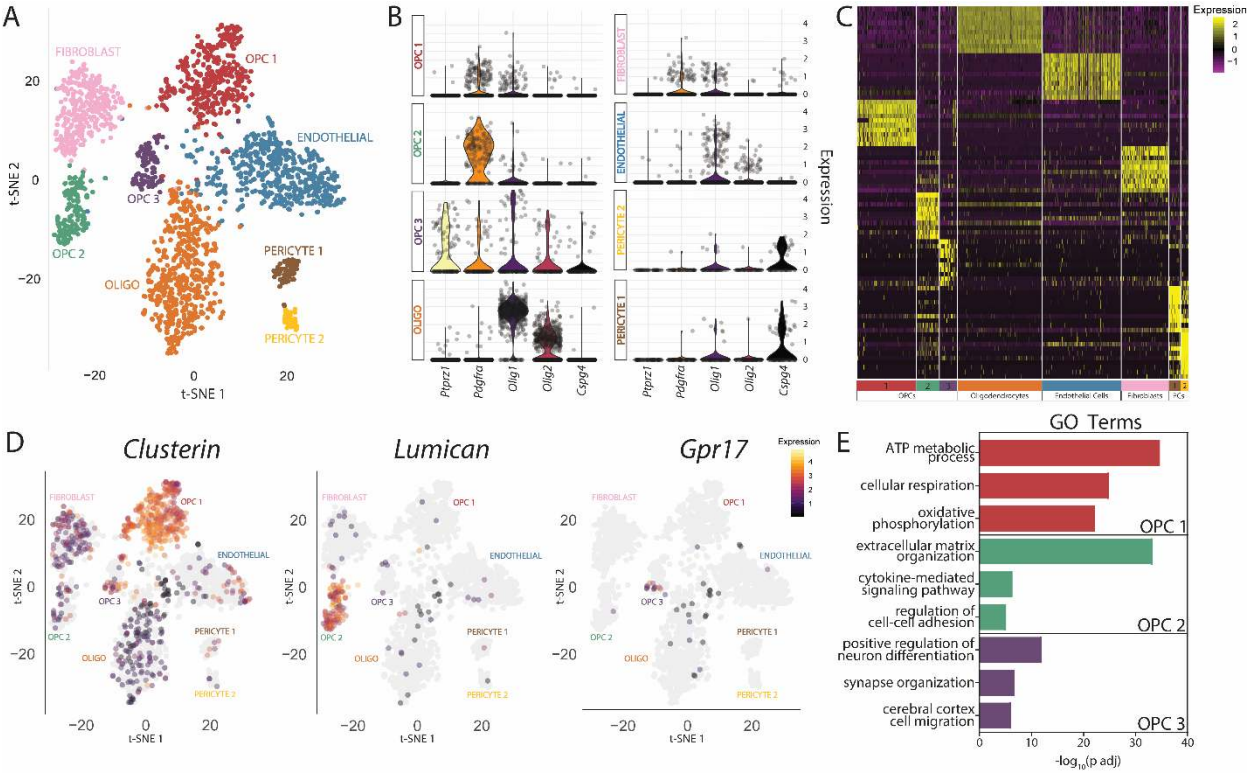

Figure 2

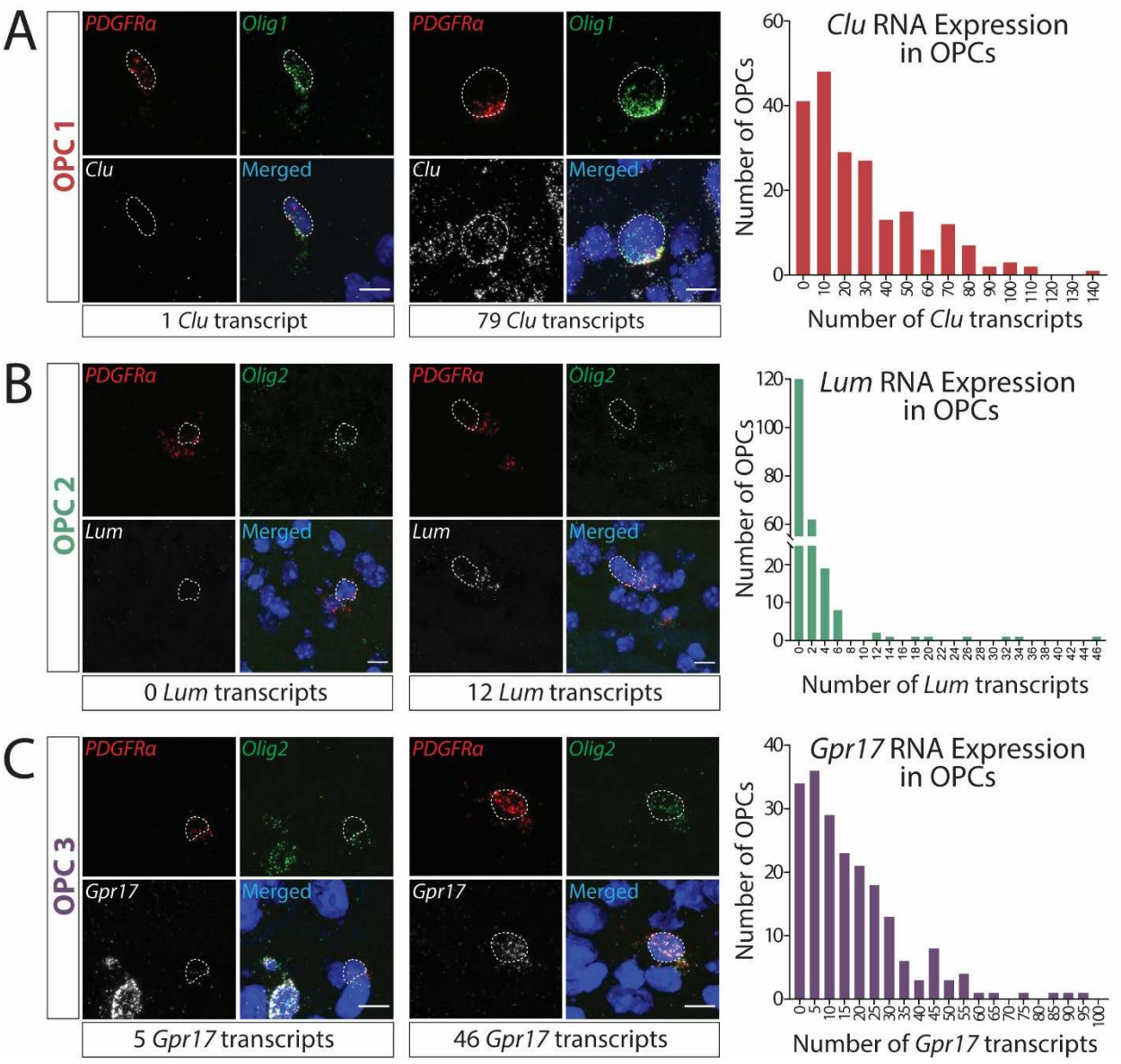

Figure 3

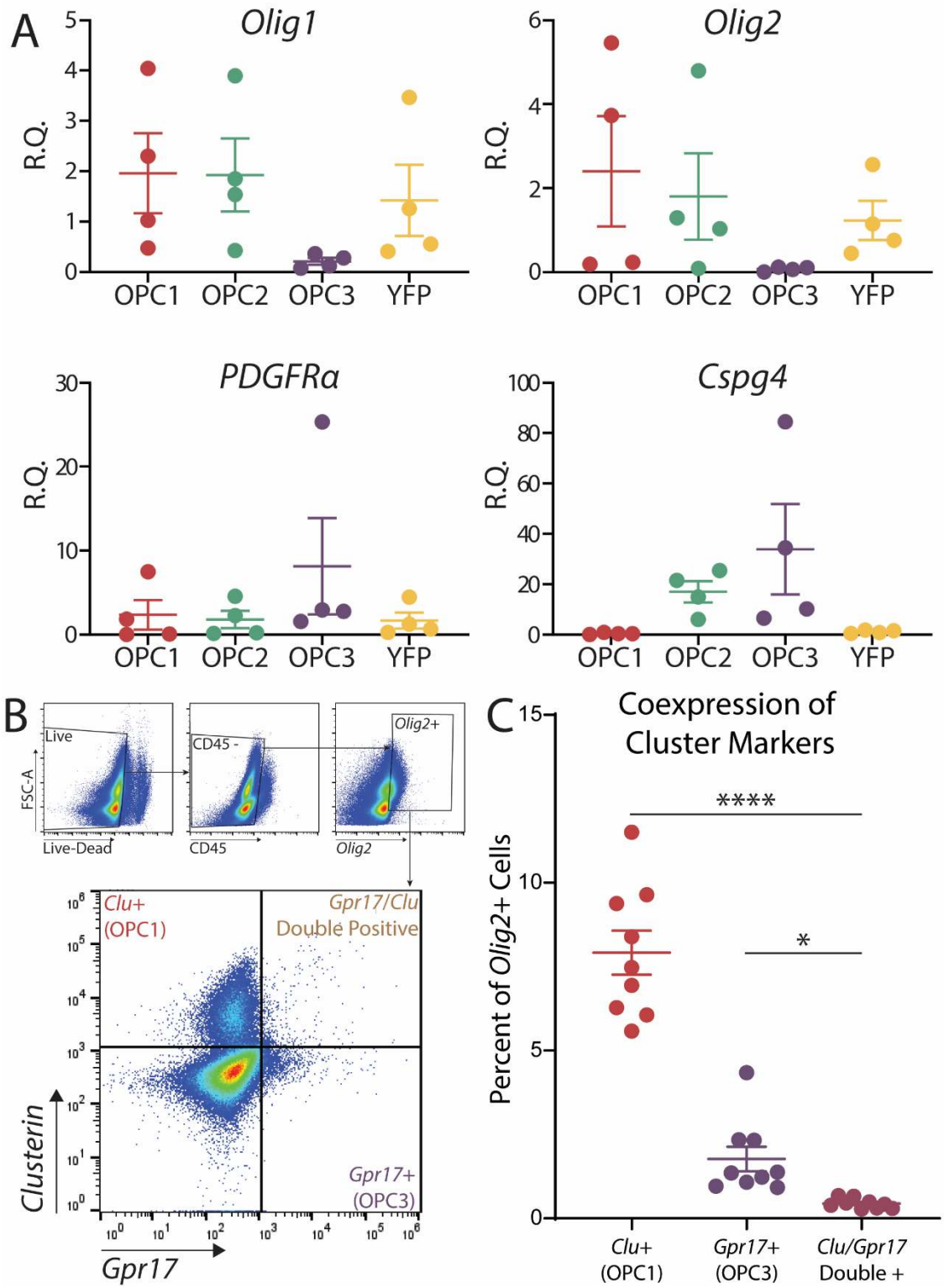

Supplemental Figure 1

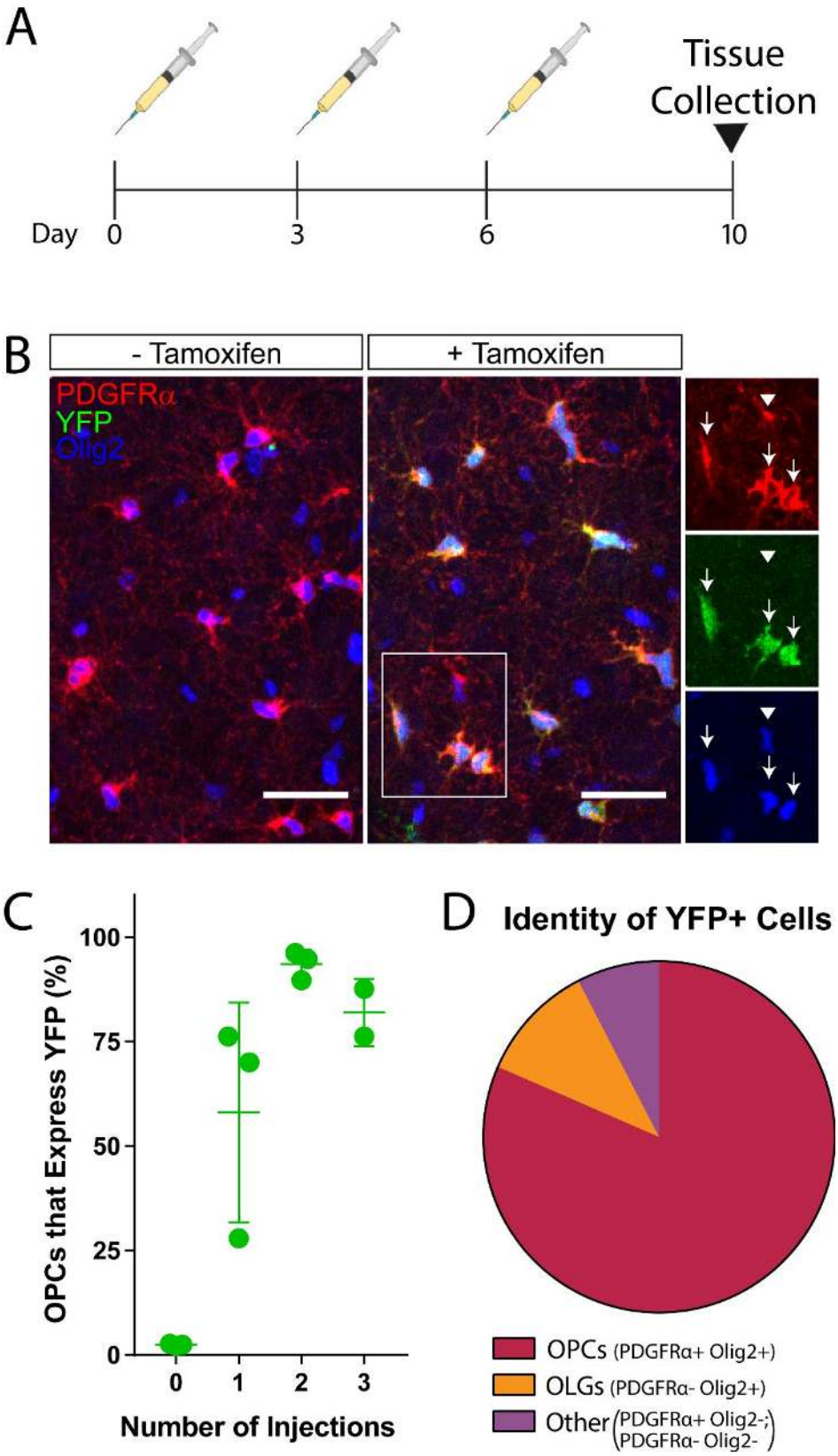

Supplemental Figure 2

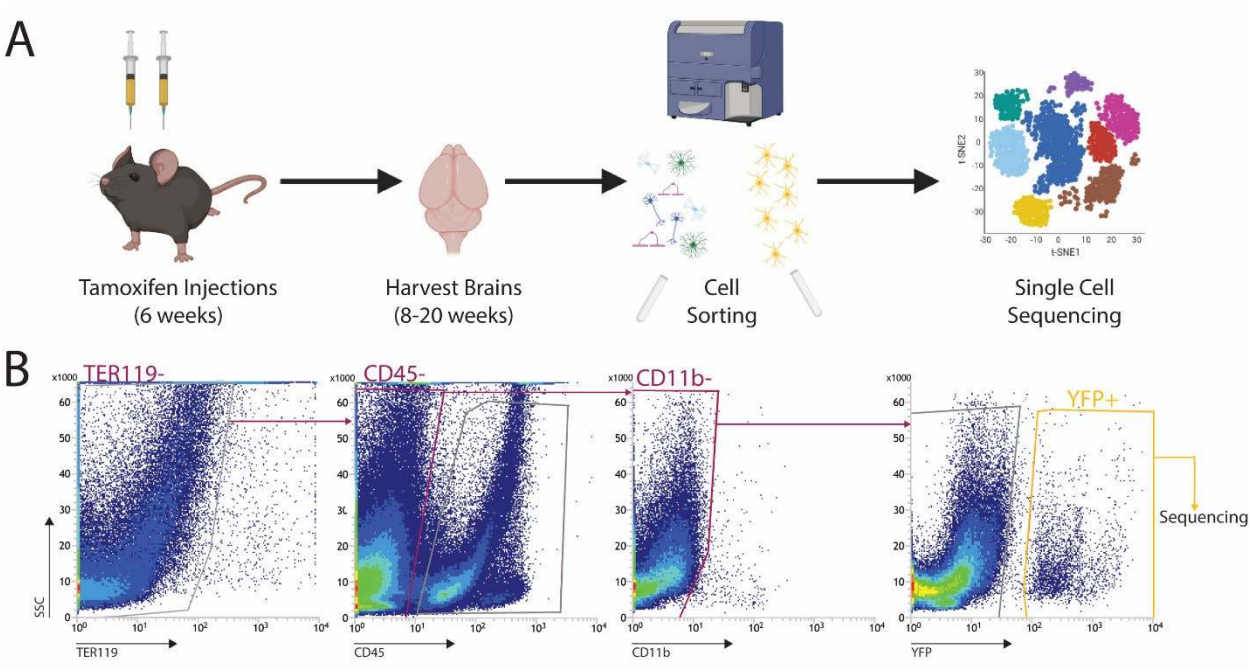

Supplemental Figure 3

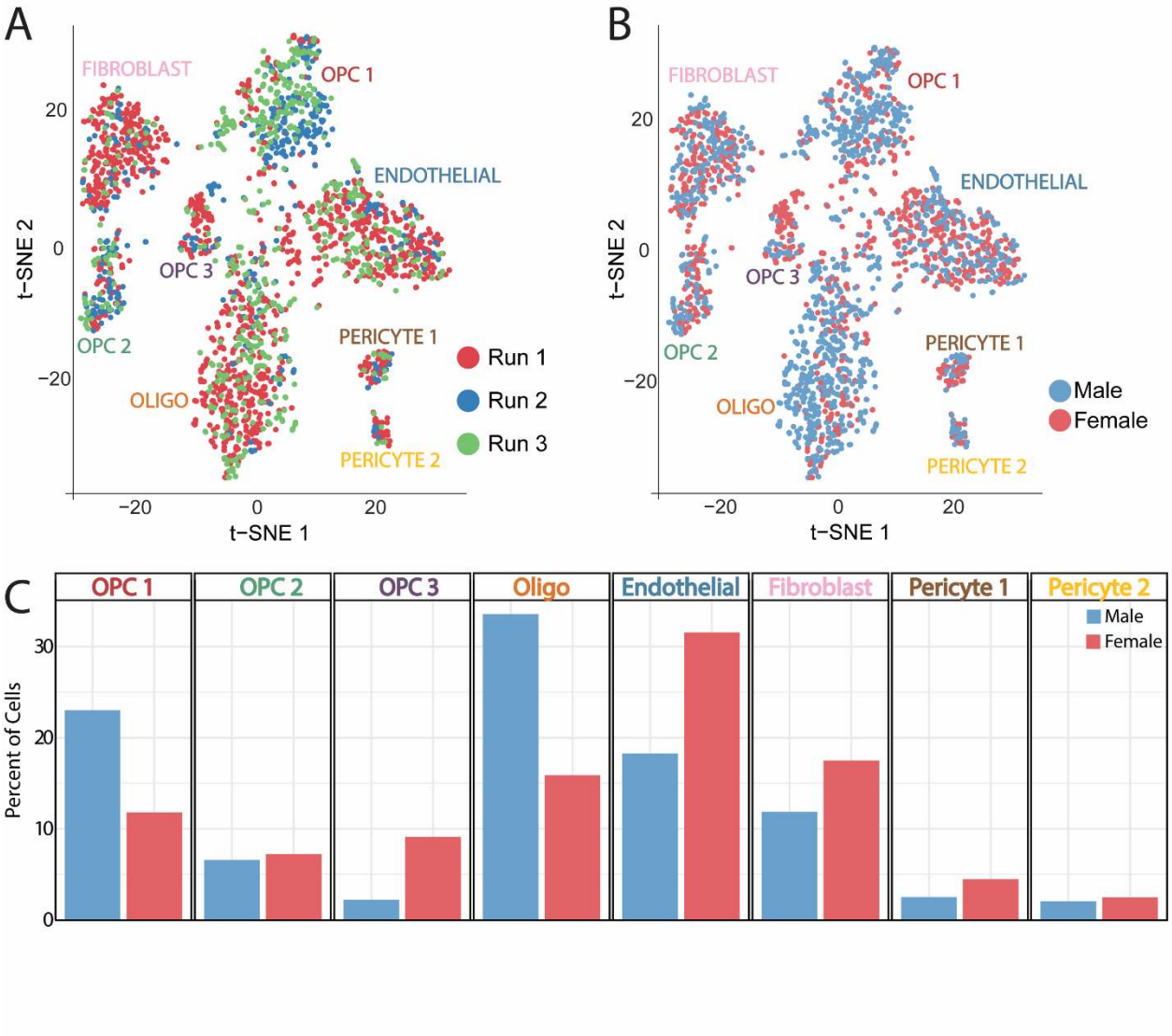

Supplemental Figure 4

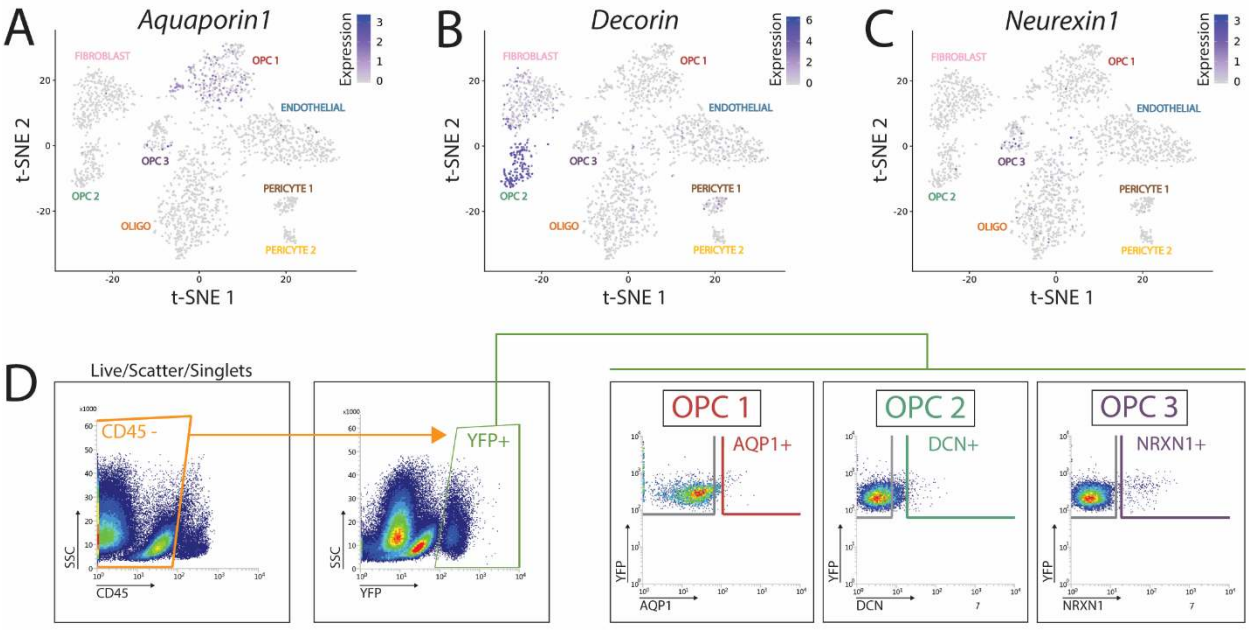

Supplemental Table 1: 60 most highly enriched genes in each OPC cluster

OPC1		
Gene	Average log-Fold Change	Adjusted p-value
Ttr	3.901936032	1.39E-211
Chchd10	2.793180871	2.60E-290
Mt3	2.724969741	1.96E-292
Enpp2	2.571921705	2.71E-204
2900040C0	2.39207625	0
Clu	2.264515279	6.72E-253
Calml4	2.058906776	0
Sostdc1	2.020727096	0
Folr1	2.019371041	0
Ppp1r1b	1.959986814	0
Atp5g1	1.939614649	1.59E-195
Spint2	1.848225166	4.48E-289
Clic6	1.812397865	0
Fxyd1	1.767568793	5.21E-225
Pcp4	1.764162682	1.60E-259
Ldhb	1.728069974	5.86E-179
Kcnj13	1.71251155	0
Igfbp2	1.704417232	3.36E-214
Kl	1.698103936	0
1500015O	1.676022595	4.62E-181
Mdh1	1.637387195	2.55E-176
Usmg5	1.601343139	9.60E-165
Hemk1	1.585765071	9.57E-280
2010107E0	1.520242307	2.62E-164
Ndufa4	1.47924378	2.28E-174
Cab39l	1.478976831	5.50E-224
Cox7b	1.472849883	1.36E-142
Ndufa1	1.453224181	2.92E-169
Prdx5	1.43900941	5.71E-148
Kcne2	1.422483955	1.86E-280
Rdh5	1.396015593	5.04E-235
Cox8a	1.385264622	2.91E-172
Atp5o.1	1.369420193	1.93E-137
Defb11	1.346478016	3.31E-268
Elob	1.334404966	2.26E-119
Atp5l	1.329250494	1.91E-157
Cox8b	1.321240543	1.22E-129
Pgk1	1.287659797	5.47E-131
Eno1	1.267669202	1.15E-129
Uqcr10	1.266134585	3.22E-132
Col9a3	1.26501598	4.20E-179
Prr32	1.258835547	8.10E-266
Apoo	1.254842615	4.38E-186
Atp5e	1.251780641	3.18E-147
Ndufa11	1.249092075	3.86E-130
Gm17018	1.248333101	1.86E-174
Slc22a17	1.241501397	1.21E-123
Uqcr11	1.233919971	1.50E-146
Gm19935	1.200990521	9.71E-228
Atp5g3	1.190597538	2.34E-117
Cox6b2	1.182789456	8.63E-144
Ndufv3	1.177414583	5.26E-114
Arl6ip1	1.16162565	6.83E-122
Smim22	1.145726157	2.07E-223
Uqcrb	1.144378814	1.17E-131
Tomm7	1.138348472	2.61E-123
Mrps6	1.137522633	8.98E-117
Uqcrq	1.133283778	7.00E-124
Cox6c	1.131404933	6.48E-155
Ndufc1	1.113267686	1.95E-106

OPC2		
Gene	Average log-Fold Change	Adjusted p-value
Dcn	4.252957397	1.09E-198
Spp1	3.151773765	4.74E-126
Apod	3.122033317	5.75E-68
Lum	2.920359913	0
Nupr1	2.518673563	7.77E-126
Itih5	2.42278495	2.22E-125
Gsn	2.38442152	1.71E-38
Slc6a13	2.381802092	1.47E-202
S100a6	2.27243541	3.52E-88
Serping1	2.270938358	2.50E-164
Cebpd	2.09527536	4.77E-51
Cxcl1	2.065038645	1.11E-62
Serpinf1	2.052267702	8.01E-154
Bgn	1.968865735	4.59E-100
Ccl2	1.934917354	6.65E-27
Pcolce	1.929435744	1.64E-84
Igfbp4	1.915877508	2.88E-99
Crispld2	1.902692084	4.72E-161
Mfap4	1.89024342	5.01E-145
Col1a1	1.888933325	3.06E-122
Olfml3	1.886209696	1.82E-145
Tgfbi	1.869526186	5.20E-91
Inmt	1.862681344	1.87E-161
Cfh	1.807268101	4.01E-119
Prelp	1.797285855	2.05E-90
Colec12	1.786707656	3.05E-233
Snhg11	1.784827073	2.46E-80
Phlda1	1.752012615	2.97E-45
Col1a2	1.719805726	3.34E-99
Edn3	1.713609982	4.65E-101
Clec3b	1.711411884	1.20E-152
Cebpb	1.67832069	5.95E-60
Pdgfra	1.676853276	4.21E-124
Col3a1	1.663723837	3.18E-151
Pam	1.630222477	2.28E-40
Cp	1.56678805	1.23E-94
Atp1a2	1.565695244	4.48E-77
Slc7a11	1.563075655	1.29E-131
Aldh1a1	1.538907037	1.85E-87
Emp1	1.529993226	2.26E-127
Timp3	1.523532559	3.22E-50
Col15a1	1.50818889	7.56E-186
Rcn3	1.504084849	3.24E-99
Cemip	1.48611691	7.25E-206
Rarres2	1.485122141	1.13E-115
Lgals1	1.484761019	3.33E-61
Lrp1	1.444164737	6.68E-67
Ifitm2	1.431830833	8.33E-59
Selenbp1	1.426342744	4.89E-105
Vcam1	1.413353519	1.09E-64
Coch	1.410260543	3.38E-34
Fam180a	1.401458771	3.01E-133
Fgfr1	1.382914159	2.09E-91
Efemp1	1.352639996	3.01E-73
Fmod	1.345067247	7.23E-25
Ctsl	1.323685493	2.25E-49
Fxyd6	1.319889862	4.67E-108
Pi16	1.312526424	5.81E-51
Hsd11b1	1.301203659	5.34E-139
Ctgf	1.300934467	1.64E-54

OPC3		
Gene	Average log-Fold Change	Adjusted p-value
Tubb2b	2.750565175	1.13E-87
Meg3	2.602122331	1.06E-62
Nnat	2.556147402	2.65E-157
Rtn1	2.382934212	1.24E-141
Fabp7	2.354098293	1.44E-43
Tubb3	2.282059611	6.14E-46
Sox11	2.185063854	2.93E-201
Gpr37l1	2.083066838	1.33E-88
Sox4	2.029870653	7.05E-47
Ccnd2	2.009175142	7.15E-23
Hmgn2	1.92825696	4.58E-11
Aldoc	1.927535012	0.00014405
Stmn2	1.901991561	2.40E-48
Tubb5	1.8965387	2.15E-09
Igfbpl1	1.893778194	3.76E-148
Basp1	1.887128477	1.32E-158
Marcksl1	1.867880033	3.90E-33
Meis2	1.848086406	4.68E-85
Cspg5	1.816439793	2.51E-30
Gm3764	1.80509589	1.65E-215
Ptprz1	1.794272071	2.52E-139
Cd24a	1.778222317	3.43E-54
Npy	1.751498349	5.65E-18
Tmsb10	1.671805939	6.82E-07
Slc1a3	1.656525106	3.35E-13
Pfn2	1.648676252	2.41E-18
Hmgb2	1.640339073	3.51E-06
Tuba1a	1.612592012	8.78E-18
6330403K0	1.598197332	5.36E-165
Hn1	1.5648415	5.21E-51
Stmn3	1.553419811	9.54E-119
Xist	1.53791178	2.02E-20
Marcks	1.535567979	1.94E-41
Celf2	1.453888057	1.64E-53
Ncam1	1.440159861	3.71E-32
Gria2	1.435714131	4.29E-97
Dcx	1.431714375	3.47E-153
Bcan	1.411910932	2.11E-88
Ntm	1.409112141	7.97E-36
Bex2	1.362657375	7.83E-53
Ppp1r14b	1.354476429	8.06E-40
Nrxn3	1.349102596	2.44E-169
Dlx6os1	1.347692313	2.14E-128
Hnrnpa1	1.336328025	9.44E-15
Celf4	1.290826736	7.40E-52
Gm17750	1.28394324	3.29E-55
Fxyd6	1.261125923	3.97E-75
Pbx1	1.258544066	8.61E-18
Hmgb3	1.251227119	6.25E-41
Nsg1	1.237314062	5.41E-56
Dlx1	1.228051311	8.93E-139
Gpm6a	1.22434178	7.25E-28
Matn4	1.209209052	2.09E-06
H2afz	1.206116964	5.21E-05
Serpine2	1.187037209	0.000252198
Gm1673	1.182518192	5.71E-25
Hist1h2ap	1.177457478	7.62E-30
Map1b	1.168622439	6.72E-09
C1ql1	1.155220203	5.50E-36
Dlx2	1.14996757	8.06E-112